Dynamics of a film bounded by a pinned contact line

J. Eggers[1], M. A. Fontelos[2]

[4]School of Mathematics, University of Bristol, Fry Building, Woodland Road, Bristol BS8 1UG, United Kingdom
[2] Instituto de Ciencias Matemáticas, (ICMAT, CSIC-UAM-UCM-UC3M), C/ Serrano 123, 28006 Madrid, Spain

(Received xx; revised xx; accepted xx)

We consider the dynamics of a liquid film with a pinned contact line (for example a drop), as described by the one-dimensional, surface-tension-driven thin-film equation $h_t + (h^n h_{xxx})_x = 0$; $h(x,t)$ is the thickness of the film. The case $n = 3$ corresponds to a film on a solid substrate. We derive an equation of motion for the contact angle $\theta(t)$, which couples to the shape of the film. Starting from a regular initial condition $h_0(x)$, we investigate the dynamics of the drop both analytically and numerically, focusing on the contact angle. For short times $t \ll 1$, and if $n \neq 3$, the contact angle changes like a power law $t^{\frac{n-2}{4-n}}$. In the critical case $n = 3$, the dynamics become non-local, and $\dot\theta$ is now of order $e^{-3/(2t^{1/3})}$. This implies that for $n = 3$, the standard contact line problem with prescribed contact angle is ill-posed. In the long time limit, the solution relaxes exponentially toward equilibrium.

1. Introduction

It is a fact universally acknowledged that the macroscopic description of a contact line can take one of two forms (Dussan V. & Chow 1983; Bonn *et al.* 2009; Wilson & D'Ambrosio 2023): the contact line may either be mobile, or stuck at a fixed position. In the mobile case, from the virtual work principle one concludes (de Gennes 1985) that the contact angle must be Young's angle, at least in equilibrium (the contact line being at rest or moving very slowly). In the pinned case, which may arise from random disorder on the surface (Bonn *et al.* 2009), or from patterning of the surface (Quéré *et al.* 2003), the contact line is stuck at a topographical or chemical barrier. In that case, the contact angle is undetermined, which one can envision as the contact line ending at a corner (Hong *et al.* 2016; Graña-Otero & Parra Fabián 2019) (cf. Fig. 1), so that a whole range of contact angles is compatible with Young's angle.

While a huge literature treats the dynamics of thin films bounded by a mobile contact line, the second case of a pinned contact line is usually examined only with regards to the conditions under which depinning occurs, i.e. when the contact starts to move again. This happens for example when a drop is placed on an incline which is sufficiently steep (Dussan V. & Chow 1983). Here instead we inquire about the nonlinear dynamics of the film while the contact line position remains fixed. For example, one can imagine placing a drop on a rough substrate, such that the contact line is always pinned. In general, the initial shape will not be an equilibrium shape, and the drop shape evolves until such an equilibrium is reached.

We will assume that transversal variations of the contact line position (e.g. contact line roughness (Bonn *et al.* 2009)), are negligible. This could also be ensured by pinning the contact line to an especially prepared, straight, and sharp-edged ridge. Moreover,

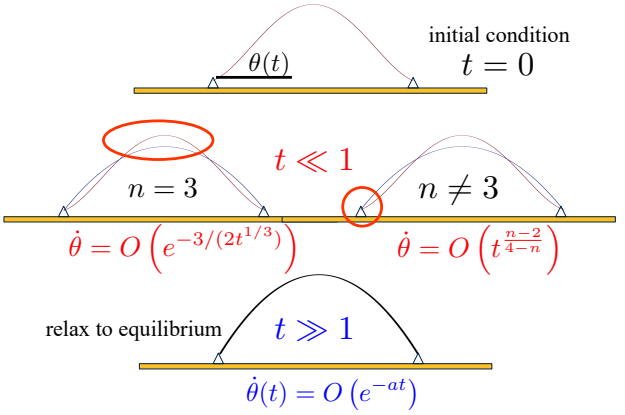

FIGURE 1. A summary of the problems considered in this paper. At some initial time $t = 0$, a drop is deposited with some arbitrary shape (here assumed symmetric), and which is pinned between two sites. At early times $t \ll 1$, the dynamics are local if $n \neq 3$ (right). If $n = 3$ (left), the motion of the contact line is driven from regions far away from the contact line. Finally, for long times, the contact angle, and the entire drop relaxes toward a quadratic equilibrium shape.

we assume that the liquid film is flat, so that the lubrication or thin-film approximation is valid. Within this framework, we will show that the contact angle is determined self-consistently through a coupling to the film profile $h(x, t)$ away from the contact line.

We assume that all lengths and time have been made dimensionless, for example using the width of the fluid film, and the capillary speed γ/η, where γ is the surface tension coefficient, and η the viscosity. Then the Laplace pressure condition at the interface requires that $p = -h_{xx}$ is the pressure inside a sliver of fluid. The flow being driven by pressure gradients p_x, the fluid flux is $f = h^n p_x$, where h^n is known as the mobility. The mobility measures the viscous resistance to the flow, which depends on the geometry and other physical effects present. Finally applying mass conservation $h_t + f_x = 0$, we arrive at the thin film equation

$$h_t + (h^n h_{xxx})_x = 0, \quad n > 0, \tag{1.1}$$

which has been used very successfully to describe the evolution of thin layers of viscous fluid (Oron *et al.* 1997; Bonn *et al.* 2009).

To name a few relevant applications of (1.1), the case $n = 3$ describes a layer of viscous fluid on a solid substrate. If fluid is allowed to slip partially over the solid surface, $n < 3$, with $n = 2$ in the most popular case of a Navier slip law (Oron *et al.* 1997; Eggers & Fontelos 2015). Strictly speaking, (1.1) then consists of two terms with powers $n = 2$ and 3: λh^2 and h^3, where λ is the slip length; here we restrict ourselves to keeping a single lower order term, which dominates near a contact line. For the rest of this paper, we will assume that the contact line is fixed at $x = 0$, while the fluid occupies some region $x > 0$. For small slopes, the contact angle is then given by $\theta(t) = h_x(0, t)$. For simplicity, we treat the representative problem of a two-dimensional drop or strip of fluid of finite width.

Starting from a smooth but otherwise arbitrary initial condition, we investigate the dynamics of a drop which eventually relaxes toward an equilibrium profile, which is quadratic in the thin film approximation. In the next section, we will derive the equation of motion for $\theta(t)$, which is coupled to the dynamics of the fluid film. We will then

describe a numerical method, based on (1.1), to describe the dynamics of the free surface of the drop, from early times until equilibrium is reached.

In the third section, we demonstrate that the early-time dynamics of the contact angle can in fact be described by a linearized equation of motion. This insight is used to find a local similarity solution describing the contact angle for early times, assuming $n \neq 3$. The degenerate, but physically most relevant case $n = 3$ is treated in following section four. The solution now consists of several regions, which are treated separately and subsequently matched together. Section five briefly describes relaxation of the drop toward equilibrium. A pictorial overview of the cases considered is shown in Fig. 1. We close with a discussion, paying particular attention to the relevance of our results to Huh and Scriven's contact line paradox (Huh & Scriven 1971). Some details of calculations are found in an Appendix.

2. Dynamics of the contact line and numerical method

We consider the evolution of a profile $h(x,t)$, as described by (1.1), which for simplicity we assume symmetric. The edges of this "drop" are pinned at $x = 0$ and $x = 2$, respectively (and after appropriate scaling). The boundary condition at $x = 0$ is $h(0,t) = 0$, while at the point of symmetry $h_x(1,t) = h_{xxx}(1,t) = 0$. For convenience let us write $n = 3 - \delta$, so that $\delta = 0$ refers to the critical case $n = 3$. To find the equation of motion for θ, we have to find the term which balances the first term in $h_t(x,t) = \dot{\theta}x + O(x^2)$. This leads to the expansion

$$h = \theta x + bx^2 \ln x + cx^2,\ \delta = 0; \quad h = \theta x + \frac{b}{\delta}x^{2+\delta} + \left(c - \frac{b}{\delta}\right)x^2,\ \delta \neq 0; \tag{2.1}$$

we have written the case $\delta \neq 0$ such that the case $\delta = 0$ emerges in the limit. Now the contact angle follows the equation of motion

$$\dot{\theta} = -2(2+\delta)(1+\delta)\theta^3 b, \tag{2.2}$$

which is $\dot{\theta} = -4\theta^3 b$ for the critical case $n = 3$. This introduces a nonlinear coupling between the contact angle and the shape of the drop, closing the system of equations to be solved. Curiously, we are not aware of (2.2) having been written down before.

In the limit of long times, we expect the drop to converge toward the equilibrium profile

$$h_{eq} = \frac{3V}{4}x(2-x), \tag{2.3}$$

fixed uniquely by the drop volume V and the drop being confined between 0 and 2.

2.1. *Numerics*

Our numerical scheme follows others used previously to solve the highly nonlinear thin film equation (Dupont *et al.* 1993; Eggers & Fontelos 2015): we use a fully explicit finite difference scheme with a staggered grid. To that end, (1.1) is split as

$$h_t + (h^{n-1}f)_x = 0, \quad f = hh_{xxx}, \tag{2.4}$$

and the interval $[0,1]$ is divided into grid points $x_i, i = 1 \ldots k$, with $x_1 = 0$ and $x_k = 1$; f is defined at the midpoints. The profile h_i is used to compute $p_k = h_{xx}$ at the grid points. At the right end we impose symmetry of h, and antisymmetry of f. The values $f_{i+1/2}$ are calculated from p_i using centered differences, p_i calculated with a 5-point scheme, valid for arbitrary grid spacings. The values of f and f_x, needed at the grid points for the first equation, are also calculated with second order accuracy.

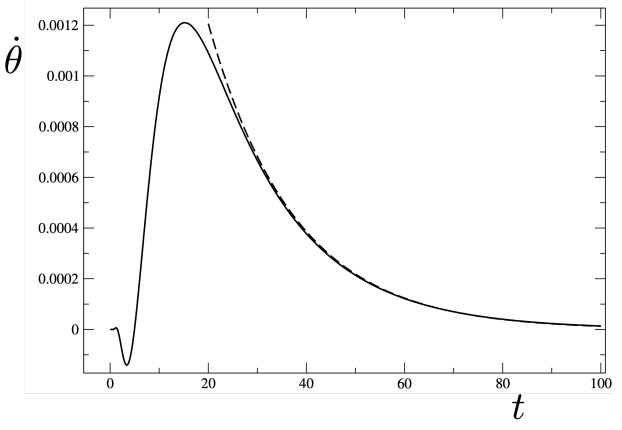

FIGURE 2. The change in contact angle $\dot\theta$ as a function of time from a numerical solution of (1.1) with $n = 3$ and initial condition $h_0(x) = \bar h \sin(\pi x/2)$, $\bar h = 0.1$. Thus, $V = 4\bar h/\pi$. For long times, $\dot\theta$ decays like e^{-t/λ_1} to zero, with $\lambda_1 = 8.19$, see section 5 below; this exponential decay is shown as the dashed line. For short times, on the other hand, θ appears to remain constant for some time ($\dot\theta = 0$); below we show that rather $\dot\theta$ behaves like $e^{-3/(2t^{1/3})}$.

Near the contact line, we impose the expansion (2.1), where the contact angle θ is a separate variable (which takes the place of v_1), and which evolves according to (2.2). The value of v_1, between x_1 and x_2, is calculated from (2.1). Likewise, for a given θ, the coefficients b and c are found from equating (2.1) to h_2 and h_3 at x_2 and x_3, respectively. Then if we let $\Delta = x_2$, and $x_3 = 2\Delta$, we find

$$b = \frac{1}{\Delta \ln 2}\left(\frac{\theta}{2} - \frac{h_3 - 4h_2}{4\Delta}\right), \quad c = -b\ln\Delta + \frac{1}{\Delta}\left(\frac{h_2}{\Delta} - \theta\right). \tag{2.5}$$

In summary, the variables are $h_2, \ldots, h_{k-1}$, $v_2, \ldots, v_{k-1}$, and θ: a total of $2k - 4 + 1 = 2k - 3$. The equations are the first of (2.4), evaluated at $x_2, \ldots, x_{k-1}$, and the second of (2.4), evaluated at $x_{1/2}, \ldots, x_{k-1/2}$, with the extra equation (2.2).

We use a strongly graded grid, with the smallest (constant) grid spacing near $x = 0$, and which is slowly increased away from $x = 0$, until a maximum spacing of 10^{-3} is reached. Our numerical scheme is fully implicit, and second order in time, using a step-halving method. Comparison between the two steps serves to adjust the time step, in order to maintain sufficient temporal resolution.

3. Early time dynamics

We begin looking at very early times after the drop has been set down. Although the original equations (1.1),(2.2) are highly nonlinear, for very early times the equations are effectively linear, as we show now.

3.1. *Effective linear dynamics*

We assume that the initial condition can be expanded into a power series of the form

$$h_0 = a_0 x + b_0 x^2 + c_0 x^3 + O(x^4). \tag{3.1}$$

Since x is small close to the contact line, we can view $c_0 x^3$ as a small perturbation to the equilibrium profile $h_{eq} = a_0 x + b_0 x^2$, around which we linearize by writing by writing

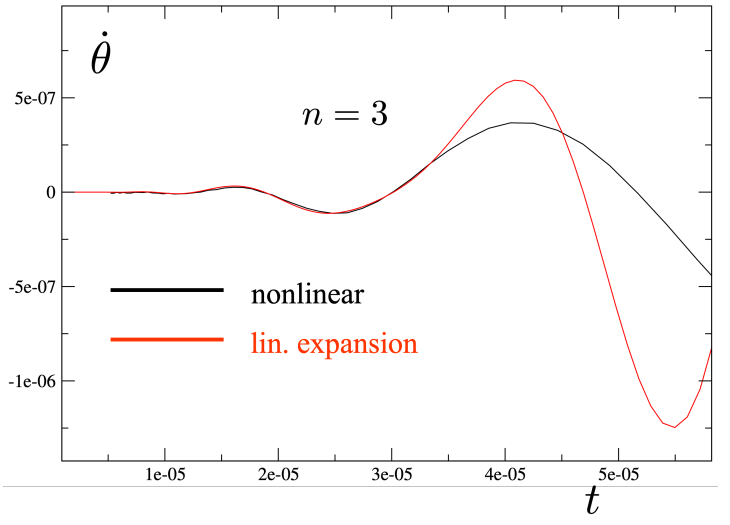

FIGURE 3. The change in contact angle $\dot{\theta}(t)$ as function of time. Black solid line: solution of (1.1) with $n = 3$ and initial condition $h_0(x) = x(2-x)+0.1x^2(2-x)^2$; contact angle found from (2.2). Boundary conditions are $h(0,t) = 0$ and $h_x(1,t) = h_{xxx}(1,t) = 0$. Red solid line: solution of the linearized leading-order equation (3.2) with $h_{eq} = 2x$ and initial condition $\delta h(x,0) = -0.4x^3$. Boundary conditions for the linearized problem are $\delta h(0,t) = 0$ and $\delta h(1,t) = 1, \delta h_{xx}(1,t) = 1$.

$h(x,t) = h_{eq}(x) + \delta h(x,t)$. We thus consider the linear equation

$$\delta h_t + \left(h_{eq}^n \delta h_{xxx}\right)_x = 0; \tag{3.2}$$

we have confirmed numerically that the early time behavior of (3.2) is indeed the same as that of the full equation.

In a second step, we argue that close to the contact line h_{eq}^n is dominated by the linear term $h_{eq} \approx a_0 x$; rescaling, we can normalize a to unity to obtain

$$\delta h_t + \left(x^n \delta h_{xxx}\right)_x = 0; \tag{3.3}$$

a linear and homogeneous problem. As the initial condition for δh, we can take the leading order expression $c_0 x^3$ of the perturbation to h_{eq} in (3.1), which amounts to $\delta h = x^3$ after initialization. In addition, we need to supply effective boundary conditions for δh; we choose

$$\delta h(1,t) = 1, \quad \delta h_{xx}(1,t) = 1, \tag{3.4}$$

which serves to set effective length and pressure scales for the problem.

The linearized form of the equation of motion for the contact angle (2.2) is

$$\dot{\theta} = -2(2+\delta)(1+\delta)b, \tag{3.5}$$

with b once more defined by (2.1), but with θ now representing the deviation of the contact angle $\delta\theta = \theta - a_0$ from its initial value. The validity of these approximations is tested in Fig. 3 for the critical case $n = 3$. As the black line, we show a simulation of the fully nonlinear equation (1.1) with contact angle condition (2.2) and boundary conditions $h(0,t) = 0$, $h_x(1,t) = h_{xxx}(1,t) = 0$. This is compared to the linearized equation (3.2), in which we have also replaced h_{eq} by the leading order expansion $h_{eq} = 2x$ of the initial condition. The initial condition of the linearized problem $\delta h(x,0) = -0.4x^3$ is derived from the cubic term of $h_0(x) = x(2-x) + 0.1x^2(2-x)^2$. For early times, excellent agreement is found, showing that the linearized leading-order approximation (3.3) fully

captures the initial growth of $\dot{\theta}$. As a result, we will base our analysis of early time dynamics on (3.3).

To remove unnecessary constants, in our analysis of (3.3) we found it useful to take the second derivative of (3.3), obtaining an equation for the curvature $\kappa = \delta h_{xx}$ of the perturbation:

$$\kappa_t + \left(x^{3-\delta}\kappa_x\right)_{xxx} = 0, \tag{3.6}$$

with initial condition $\kappa = 6x$. From (2.1) we find that for small x,

$$\kappa = \frac{(2+\delta)(1+\delta)b}{\delta}x^\delta + 2\left(c - \frac{b}{\delta}\right),\ \delta \neq 0, \quad \kappa = 2b\ln x + 3b + 2c,\ \delta = 0. \tag{3.7}$$

Inserting the initial condition into (3.6), we obtain $\kappa_t = -6(3+\delta)(2+\delta)(1+\delta)x^\delta$, so that at short times the solution is

$$\kappa = 6x - 6(3+\delta)(2+\delta)(1+\delta)x^\delta t.$$

This means new terms of the form (3.7) are generated immediately, and the contact angle must change. We can expect a local solution driven by the dynamics of the contact line alone. If on the other hand $\delta = 0$, $\kappa = 6x - 36t$ solves (3.6) exactly, and is compatible with the initial conditions. The dynamics are now driven by the fact that the solution is no longer compatible with the boundary condition at the other end: a very non-local process. As a result, the contact angle hardly change initial, since the driving is extremely weak. We start with the local, generic, case $\delta \neq 0$.

3.2. *The contact angle, $\delta \neq 0$*

We begin with the case where n does not equal the generic value for a liquid film on a solid substrate. We are looking for similarity solutions of the form $\kappa = t^\gamma P(\xi)$, where $\xi = x/t^{1/(1+\delta)}$, so that (3.6) is satisfied. For large ξ, this solution has to match $\kappa = 6x$; this implies that $\gamma = 1/(1+\delta)$, so that

$$\Delta\kappa = t^{1/(1+\delta)}P(\xi), \quad \xi = x/t^{1/(1+\delta)} \tag{3.8}$$

is the form of the similarity solution, with $P(\xi) = 6\xi$ for large arguments. The similarity equation becomes

$$\frac{P - \xi P_\xi}{1+\delta} + \left(\xi^{3-\delta}P_\xi\right)_{\xi\xi\xi} = 0. \tag{3.9}$$

Four linearly independent solutions P_1, P_2, P_3,and P_4 to (3.9) can be found in terms of generalized hypergeometric functions, as given in appendix A, cf. (A 1)- (A 4); they are real for $\xi > 0$. Very similar solutions to an elastic fourth order problem have been described in (Stone & Duprat 2016). The solutions P_2 and P_4 are singular at the origin, and on account of (3.7) have to be excluded. The remaining solutions P_1 and P_3 grow exponentially at infinity, while we demand $P(\xi) = 6\xi$. As shown in detail in appendix A, we can cancel the exponential growth by superimposing P_1 and P_3. Different expressions apply for $\delta > 0$ and for $\delta < 0$, respectively. In summary, the solution to (3.9) satisfying all required conditions can be written in the form

$$P(\xi) = P_0\left(P_3(\xi) - rP_1(\xi)\right), \tag{3.10}$$

where P_0 (cf. (A 6)) is chosen such that (3.10) matches $P = 6\xi$.

For small ξ, the solution behaves as

$$P \approx P_0\left(\xi^\delta - r\right); \tag{3.11}$$

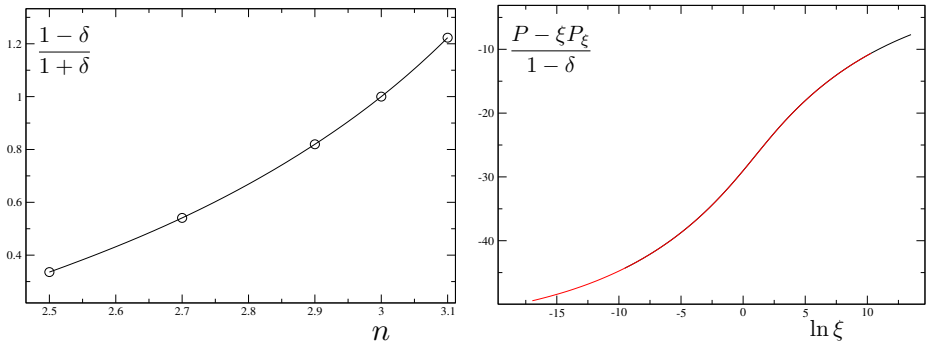

FIGURE 4. Left: numerical results for the exponent of $\dot{\theta}$, based on (3.3), compared to the analytical result (3.12) (solid line). Right: numerical result for the first term in (3.9) as a function of $\ln\xi$ (black solid line, $\delta = 0.1$) compared to the analytical solution (3.10) (red solid line).

comparing to (3.7), and using (3.5) we find

$$\dot{\theta} = -2a_0^3\delta P_0 t^{\frac{1-\delta}{1+\delta}} \tag{3.12}$$

and

$$c = \frac{P_0}{(2+\delta)(1+\delta)} t^{\frac{1-\delta}{1+\delta}} - \frac{P_0 r}{2} t^{\frac{1}{1+\delta}}. \tag{3.13}$$

This means that as the drop is set down, the contact angle changes immediately according to (3.12). This is tested by comparison to numerical simulations of the the linearized equation (3.3) for $n \neq 3$. On the left of Fig. 4, we show the exponent of $\dot{\theta}$. The solid line is $(1-\delta)/(1+\delta)$ as found from (3.12). The symbols are the exponent as found from numerical simulations. On the right of Fig. 4, the left hand side of (3.9) (as determined numerically, black solid line), is tested against the analytical solution (3.10) (red solid line), and perfect agreement is found.

Strictly speaking, the similarity solution (3.10) is only one of an infinite sequence of solutions of higher order, but which are unstable (Eggers & Fontelos 2015). If the initial condition happens to be such that the coefficient of x^3 vanishes exactly, one must consider the next order, x^4, or an exponent $n \geqslant 3$ in general. However, an arbitrarily small perturbation will generate a term proportional to x^3, rendering solutions of higher order unstable. In that case the asymptotic behavior is $P \propto \xi^{n-2}$, and the (higher-order) similarity solution is of the form

$$\Delta\kappa = t^{(n-2)/(1+\delta)} P(\xi), \quad \xi = x/t^{1/(1+\delta)}, \tag{3.14}$$

with similarity equation

$$\frac{(n-2)P - \xi P_\xi}{1+\delta} + \left(\xi^{3-\delta} P_\xi\right)_{\xi\xi\xi} = 0. \tag{3.15}$$

The two solutions with the correct behavior at the origin (given in appendix A, cf. (A 7)) can again be superimposed to generate a solution that behaves like ξ^{n-2} at infinity, as required.

4. The contact angle, $\delta = 0$

Let us summarize the situation for the special case $n = 3$, which corresponds to a no-slip condition. The linearized equation for $\delta h(x,t)$ is

$$\delta h_t + \left(x^3 \delta h_{xxx}\right)_x = 0, \tag{4.1}$$

which we are solving with the initial condition $\delta h_0(x) = \delta h(x,0) = x^3$. The boundary conditions are $\delta h(0,t) = 0$, $\delta h(1,t) = 1$, and $\delta h_{xx}(1,t) = 6$.

The linearized equation for $\delta h_{xx} = \kappa$ is now

$$\kappa_t + \left(x^3 \kappa_x\right)_{xxx} = 0, \tag{4.2}$$

and to leading order near the contact line, δh and δh_{xx} are of the form

$$\delta h = \theta x + b x^2 \ln x + c x^2, \quad \kappa = 2b \ln x + 3b + 2c, \tag{4.3}$$

and the equation for the change in contact angle is $\dot{\theta} = -4b$. Taking into account (4.3), this constitutes a complete set of boundary conditions. Remember that in the linearized version, θ corresponds to the deviation of the contact angle from the equilibrium value, and the initial condition is $\theta = 0$.

A new feature of the case $\delta = 0$ is that there is an exact solution of (4.1) and (4.2):

$$\delta h_{ex}(x,t) = x^3 - 18 t x^2, \quad \kappa_{ex}(x,t) = 6x - 36t, \tag{4.4}$$

which also satisfies the initial conditions, as well as the boundary condition at the contact line. However, for $t > 0$ it violates the boundary conditions $\delta h(1,t) = 1$ and $\delta h_{xx}(1,t) = \kappa(1,t) = 6$ at the right end of the domain. As a result, the dynamics starts from the right of the domain, and propagates toward the contact line.

It is advantageous, in particular for the numerics, to formulate everything in terms of the deviations

$$\Delta h = \delta h - \delta h_{ex}, \quad \Delta\kappa = \kappa - \kappa_{ex}, \tag{4.5}$$

in order to avoid rounding error. Then the equations of motion (4.1), (4.2) remain the same, as well as the boundary condition at the contact line. On the boundary $x = 1$, on the other hand, we now have to satisfy

$$\Delta h(1,t) = 18t, \quad \Delta h_{xx}(1,t) = 36t. \tag{4.6}$$

Also, the expansions (4.3) remain valid:

$$\Delta h = \theta x + b x^2 \ln x + c x^2, \quad \Delta\kappa = 2b \ln x + 3b + 2c, \tag{4.7}$$

except that the constant c has changed its meaning.

Figure 5 illustrates the particular situation in the singular case $\delta = 0$, in which (4.4) is a solution to the problem, but where the boundary conditions (3.4) are violated. As a result, a localized "pulse" is created near $x = 1$, which grows in time. We start by looking for a similarity solution describing the localized growth of the pulse. There is a corresponding similarity solution at the contact line $x = 0$ itself, which is driven by the pulse. As a result, it is of a much smaller amplitude, not visible on the scale of Fig. 5. We will call that the contact line solution. We will see that the two solutions do not match directly, so we need to construct an intermediate solution which connects the two.

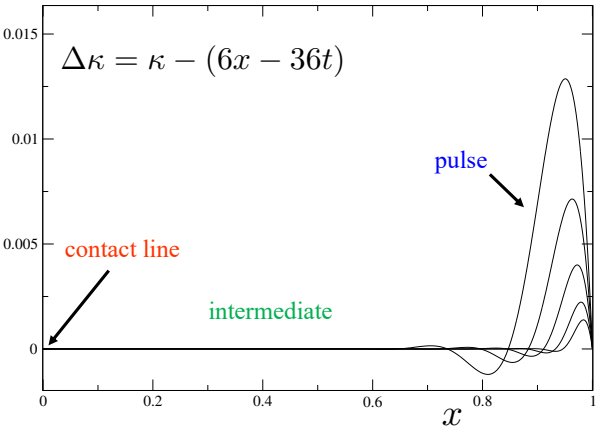

FIGURE 5. A sequence of profiles $\Delta\kappa$ for times $\log_{10} t = -7.5, -7, \ldots, -4$, from a numerical solution of (3.3), with $n = 3$. A localized "pulse" solution grows at the right boundary, which excites a "contact line" solution at $x = 0$, but with an amplitude that is exponentially damped. The two solutions are connected by an intermediate solution.

4.1. *Similarity solution near $x = 1$: the pulse solution*

To understand the origin of the oscillations which are generated at the right end of the interval, we consider the similarity solution

$$\Delta\kappa = t^\alpha \phi(\zeta), \quad \zeta = \frac{1-x}{t^{1/4}}, \tag{4.8}$$

located at $x = 1$. The exponent $1/4$ follows from (4.2), considering that $x \approx 1$, while $\alpha = 1/2$ follows from $\delta h_t = -\delta h_{xxxx} = -\Delta\kappa_{xx}$ and $\delta h(1,t) = 18t$, so that $\Delta\kappa_{xx}(1,t) = -18$. We thus have

$$\Delta\kappa = t^{1/2} \phi(\zeta), \quad \zeta = \frac{1-x}{t^{1/4}}, \tag{4.9}$$

where ϕ satisfies the similarity equation

$$\frac{\phi}{2} - \frac{\zeta\phi'}{4} + \phi^{iv} = 0. \tag{4.10}$$

Four linearly independent solutions ϕ_1, ϕ_2, ϕ_3, and ϕ_4 are given in (B 1); of them, ϕ_3 does not satisfy $\phi(0) = 0$, required to conform with the boundary condition $\kappa(1,t) = 6$, and drops out. In addition, we want ϕ to decay at infinity. As explained in more detail in appendix B, the ratio between the two remaining hypergeometric functions is fixed to $r = \sqrt{2}\pi/(24\Gamma^2(3/4))$, so that the exponential growth cancels. In a second step, we fix the amplitude of ϕ_3 to $r_1 = \pi/(4\Gamma(3/4))$ to remove the term growing quadratically at infinity. The remaining combination then decays exponentially at infinity. This leaves us with the solution

$$\phi = A\left[\zeta_1 \mathrm{F}_3\left(-\frac{1}{4}; \frac{1}{2}, \frac{3}{4}, \frac{5}{4}, \frac{\zeta^4}{256}\right) + \frac{\sqrt{2}\pi}{24\Gamma^2\left(\frac{3}{4}\right)}\zeta^3 {}_1\mathrm{F}_3\left(\frac{1}{4}; \frac{5}{4}, \frac{3}{2}, \frac{7}{4}, \frac{\zeta^4}{256}\right) - r_1\zeta^2\right], \tag{4.11}$$

which behaves like $\phi \approx A\zeta - r_1\zeta^2$ for small ζ. To finally fix A we observe that the boundary condition at $x = 1$ is $-18 = \Delta\kappa_{xx}(1,t) = \phi''(0) = -2Ar_1$, from which $A = 9/r_1 = 36\Gamma(3/4)/\pi \approx 14.0422$. This fixes all parameters of the pulse solution (4.11), which is shown as the dashed line in Fig. 6. Clearly, very good agreement with numerical simulation is found, without an adjustable parameter.

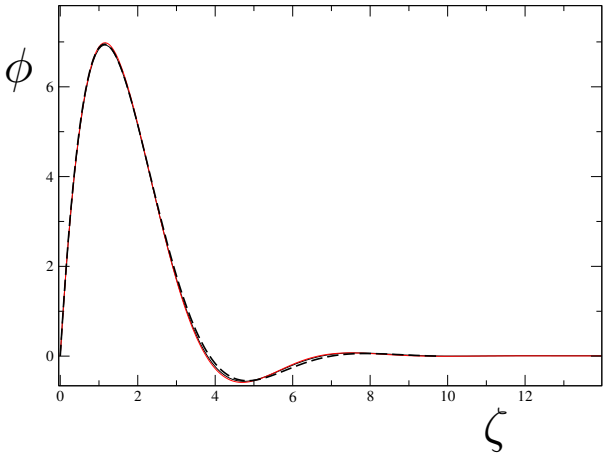

FIGURE 6. The profile ϕ as found from computing $\Delta\kappa$, rescaled according to the similarity solution (4.9), for $t = 3.2 \cdot 10^{-8}$ (black line) and $t = 10^{-7}$ (red line). The dashed line is the solution (4.11).

To understand the behavior for large ζ (away from the corner), we make the WKB ansatz $\phi \propto e^{S(\zeta)}$. Inserting into (4.10), to leading order we get $-\zeta S'/4 + S'^4 = 0$, or

$$S' = \left(\frac{\zeta}{4}\right)^{1/3} \begin{cases} 1 \\ -1/2 + \sqrt{3}i/2 \\ -1/2 - \sqrt{3}i/2 \end{cases},$$

where the last two solutions are the relevant case which decays for large ζ. Integrating, we obtain

$$S_{1/2} = S_0 - \frac{3\zeta^{4/3}}{2 \cdot 4^{4/3}}(1 \pm \sqrt{3}i). \tag{4.12}$$

To capture algebraic corrections, we need to go to next order:

$$S' = \left(\frac{\zeta}{4}\right)^{1/3} \left(-\frac{1}{2} \pm \frac{\sqrt{3}i}{2}\right) + \epsilon \equiv P + \epsilon,$$

for which the leading terms in (4.10) are

$$\frac{1}{2} - \frac{\zeta S'}{4} + S'^4 + 6S''S'^2 = 0,$$

so that $\epsilon = -4/(3\zeta)$. The complex roots can be combined to cosine and sine modes, so that the asymptotic solution finally becomes

$$\phi \approx A_p \zeta^{-4/3} e^{-\frac{3\zeta^{4/3}}{2 \cdot 4^{4/3}}} \cos\left(\frac{3^{3/2}\zeta^{4/3}}{2 \cdot 4^{4/3}} - \phi_p\right). \tag{4.13}$$

Here $\phi_p = 0.561$ is a phase factor, and the amplitude is $A_p = 3.6599A \approx 51.39316$, both found numerically, based on a numerical evaluation of (4.11), using MAPLE. This means that Δp near the right end of the domain is

$$\Delta\kappa \approx A_p t^{1/2} \zeta^{-4/3} \exp\left[-\frac{3\zeta^{4/3}}{2 \cdot 4^{4/3}}\right] \cos\left(\frac{3^{3/2}\zeta^{4/3}}{2 \cdot 4^{4/3}} - \phi_p\right). \tag{4.14}$$

4.2. *Similarity solution near the contact line*

Note that (4.12) implies

$$S_{1/2} \propto (1 \pm \sqrt{3}i)\frac{(1-x)^{4/3}}{t^{1/3}}, \tag{4.15}$$

which suggests a similarity solution of the form

$$\Delta\kappa = e^{-\frac{\mu}{\alpha t^\alpha}} A(\xi), \quad \xi = \frac{x}{t^{1+\alpha}}, \tag{4.16}$$

where μ is expected to be complex, and α real. We will find $\alpha = 1/3$ corresponding to (4.12), but will at first continue the calculation for general α; note that A is also complex.

Inserting (4.16) into (4.2) we obtain

$$\mu A - (1+\alpha)t^\alpha \xi A' + \left(\xi^3 A'\right)''' = 0,$$

which for $\alpha > 0$ and $t \to 0$ simplifies to

$$\mu A + \left(\xi^3 A'\right)''' = 0. \tag{4.17}$$

Of the four solutions to (4.17) given in (C 1), A_3 and A_4 are singular at the origin, and are therefore excluded. Instead, we are looking for solutions which are consistent with (4.3) at the origin.

As shown in Appendix C, the leading-order exponential behavior of the remaining two solutions is

$$A_1 \sim e^{4i(-\mu)^{1/4}\xi^{1/4}}, \quad A_2 \sim e^{4(-\mu)^{1/4}\xi^{1/4}}. \tag{4.18}$$

We will see by matching to the intermediate solution that only A_1 has the correct behavior at infinity, and thus is the only solution to be considered. Its asymptotic behavior at the origin can be evaluated very efficiently using Barnes-type integral representations, as detailed in Appendix C, and resulting in

$$A_1 = -\frac{\ln(-\mu\xi)}{2} + \frac{5}{4} - 2\gamma + O(\xi, \xi\ln\xi), \tag{4.19}$$

at leading order.

4.3. *The intermediate solution*

We are still missing an intermediate solution which connects the solution (4.16) with A given by (C 4), to the pulse solution (4.9) with ϕ given by (4.11). In the process, we hope to find the parameters α, μ of the contact line solution. On the one hand, the tail of the pulse solution (4.15) has a space dependence $e^{(1-x)^{4/3}}$, while on the other hand (4.18) implies $e^{x^{1/4}}$, which clearly is not the same.

The required solution, which fits both asymptotic behaviors, is given by

$$\Delta\kappa = e^S, \quad S = -\frac{G(x)}{t^{1/3}}, \tag{4.20}$$

as we will show now; the exponent $t^{1/3}$ in the denominator is motivated by (4.15). Taking S to be of order $t^{-1/3}$ and x to be of order one, the leading order expression is

$$S_t + x^3 S_x^4 = 0, \tag{4.21}$$

and so the equation for G becomes

$$\frac{G}{3} + x^3 G_x^4 = 0, \tag{4.22}$$

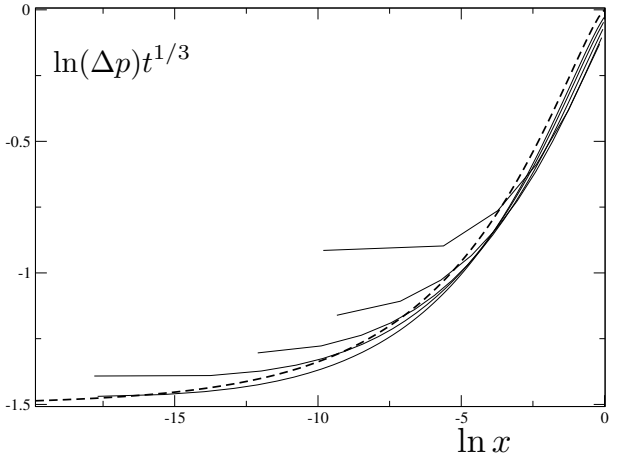

FIGURE 7. A solution of (4.1) at $\ln t = -16, -14, -12, -10, -8$. Plotted are the maxima of Δp as function of their locations. For earlier times, the profiles converge toward the amplitude of the intermediate solution (4.24), which is $3\left(1 - x^{1/4}\right)^{4/3}$.

whose solution with boundary condition $G(1) = 1$ is

$$G = 3(-1)^{1/3}\left(1 - x^{1/4}\right)^{4/3}, \tag{4.23}$$

and the roots are to be taken appropriately.

Near $x = 1$ let us put $x = 1 - s$, so that for $s \ll 1$

$$G \approx 3(-1)^{1/3}\left(\frac{s}{4}\right)^{4/3},$$

which has to match the leading order behavior (4.12), which implies

$$G \approx \frac{3}{2 \cdot 4^{4/3}}\left(1 \pm \sqrt{3}i\right) s^{4/3}.$$

Clearly, if the roots $(-1)^{1/3} = (1 \pm \sqrt{3}i)/2$ are selected, this is an exact match, so that now the solution in the intermediate region becomes

$$G = \frac{3}{2}\left(1 \pm \sqrt{3}i\right)\left(1 - x^{1/4}\right)^{4/3}. \tag{4.24}$$

This result is tested in Fig 7, by plotting $\Delta\kappa$, multiplied by $t^{1/3}$. For simplicity, we disregard the oscillations, by plotting maxima of $\Delta\kappa$ only, as function of the maximum position. Thus the real part of (4.24) is plotted as the dashed line, which agrees progressively for earlier times.

Now for $x \to 0$, (4.24) must match the large-ξ behavior of (4.18). The former limit leads to

$$\ln \Delta\kappa \sim -\frac{3}{2}\left(1 \pm \sqrt{3}i\right)\frac{1 - 4x^{1/4}/3}{t^{1/3}},$$

while the latter, using (4.18), gives

$$\ln \Delta\kappa \sim -\frac{\mu}{\alpha t^{\alpha}} + 4i(-\mu)^{1/4}\frac{x^{1/4}}{t^{(1+\alpha)/4}}.$$

It is straightforward to confirm that if we identify

$$\alpha = \frac{1}{3}, \quad \mu = \frac{1+\sqrt{3}i}{2}, \tag{4.25}$$

the two expressions become identical, having used that $(-\mu)^{1/4} = (\sqrt{3}-i)/2$. To avoid confusion, we have chosen the plus sign for μ. However, since (4.17) is a real equation, replacing μ by its complex conjugate yields another solution. While A_1 grows at the exponential rate $e^{2\xi^{1/4}}$, A_2 grows at the faster rate $e^{2\sqrt{3}\xi^{1/4}}$, and therefore does not match.

To summarize, the contact line solution is

$$\Delta\kappa = e^{-\frac{3(1+\sqrt{3}i)}{2t^{1/3}}} A_1(\xi), \quad \xi = \frac{x}{t^{4/3}}, \tag{4.26}$$

with $A_1 = \text{MeijerG}([[],[]],[[0,0],[-2,-1]],-\mu\xi)$, together with its complex conjugate. Equation (4.17) is valid under the assumption that $t^{1/3}\xi A_\xi \ll A$. Using (4.18), this implies $\xi \ll t^{-4/3}$, or x small. On the other hand, the validity of the intermediate solution relies on $G'^4/t^{4/3}$ being small in comparison to G'^2G''/t. In other words, x must be greater than $t^{4/3}$, so clearly there is an overlap for $t \to 0$.

The physical (real valued) solution based on (4.26) must be a linear superposition of real and imaginary parts. Thus putting $A_1 = A_r + iA_i$, we obtain

$$\Delta\kappa = e^{-3/(2t^{1/3})}\left[\epsilon_1\left(\cos\left(\frac{3\sqrt{3}}{2t^{1/3}}\right)A_r + \sin\left(\frac{3\sqrt{3}}{2t^{1/3}}\right)A_i\right) + \epsilon_2\left(\cos\left(\frac{3\sqrt{3}}{2t^{1/3}}\right)A_i - \sin\left(\frac{3\sqrt{3}}{2t^{1/3}}\right)A_r\right)\right. \tag{4.27}$$

Now with (4.25), $\ln(-\mu) = -2\pi i/3$, and so for small ξ

$$A_r = -\frac{\ln x}{2} + \frac{5}{4} - 2\gamma + \frac{2}{3}\ln t, \quad A_i = \frac{\pi}{3},$$

where γ is Euler's constant. This yields

$$\dot\theta = e^{-3/(2t^{1/3})}\left[\epsilon_1\cos\left(\frac{3\sqrt{3}}{2t^{1/3}}\right) - \epsilon_2\sin\left(\frac{3\sqrt{3}}{2t^{1/3}}\right)\right], \tag{4.28}$$

where ϵ_1 and ϵ_2 remain to be determined. In order to do that, we have to go to next order in the expansion. The reason is that prefactors can be interpreted as logarithmic corrections in the exponential, but which are subdominant, and require a higher order result.

4.4. *The next order*

To find the remaining amplitudes ϵ_1 and ϵ_2, we need to continue to the next order. So far we have accounted for the exponential terms, but want to capture the terms from (4.13) and (4.18) which only grow algebraically. In the spirit of (4.20), we now try the generalized ansatz (with G given by (4.24)):

$$S = G(x)t^{-1/3} + G_1(x) + g_1\ln t + g_2\ln x + g_3\ln(1-x). \tag{4.29}$$

The constants g_1, g_2, and g_3 are to be adjusted to match the required power laws.

Namely, the large-ξ expansion of A_1 (cf. (4.18)) amounts to

$$S_{in} = 2\left(1 \pm \sqrt{3}i\right)\frac{x^{1/4}}{t^{1/3}} - \frac{9}{8}\ln x + \frac{3}{2}\ln t + const, \tag{4.30}$$

while for small $s = 1 - x$ the pulse solution yields

$$S_{out} = -\frac{3\left(1 \pm \sqrt{3}i\right)}{2 \cdot 4^{4/3}} \frac{s^{4/3}}{t^{1/3}} - \frac{4}{3} \ln s + \frac{5}{6} \ln t. \tag{4.31}$$

Comparing to (4.29), and matching to $\ln t$ and $\ln s$ in the expansion for small s, we find $g_1 = 5/6$ and $g_3 = -4/3$; matching to $\ln x$ in the expansion for small x, we find $g_2 = -9/8$. Notice there is a mismatch in the contribution from $\ln t$, so (4.16) needs to be multiplied by $t^{-2/3}$, so that $3/2 - 2/3 = \alpha$ as required. This change does not alter the leading order equation (4.17), but changes only the next order.

To make everything consistent, (4.21) has to supplemented with terms of order t^{-1}, leading to

$$S_t + x^3 \left(S_x^4 + 6S_x^2 S_{xx}\right) + 9x^2 S_x^3 = 0. \tag{4.32}$$

Inserting (4.29) into (4.32), at order t^{-1} we have

$$4(1 + G_1')x^{5/4} - G_1' x^{9/4} + x(x-1)G_1' - \frac{4x}{3} + \frac{x^{1/4}}{3} = 0,$$

which can be integrated to give

$$G_1 = \frac{4}{3} \ln\left(1 + x^{1/4} + x^{1/2} + x^{3/4}\right) + const$$

This finally leads to

$$\Delta\kappa = A_{med} e^{-\frac{3}{2}\left(1 \pm \sqrt{3}i\right)\frac{(1-x^{1/4})^{4/3}}{t^{1/3}}} \frac{1 + x^{1/4} + x^{1/2} + x^{3/4}}{x^{9/8}(1-x)^{4/3}} t^{5/6} \tag{4.33}$$

in the intermediate region, where A_{med} is an amplitude to be determined. To recall, (4.33) solves (4.32) and matches inner and outer regions (4.30) and (4.31), respectively, once a correction $-2 \ln t/3$ has been added to the inner solution. This means to leading order the inner solution is now $\Delta\kappa = t^{-1/2} e^{-\frac{\mu}{\alpha t^\alpha}} A(\xi)$ instead of (4.16). This will generate an additional term in (4.17), which is proportional to $t^{1/3}$. This motivates the ansatz to include a term of next order into the inner solution:

$$\Delta\kappa = e^{-3\mu_\pm t^{-1/3}} \left[t^{-2/3} A(\xi) + t^{-1} B(\xi)\right]. \tag{4.34}$$

At leading order, this yields (4.17), as before; at the next order, we have

$$-\frac{2A}{3} - \frac{4\xi A'}{3} + \mu B + \left(\xi^3 B'\right)''' = 0, \tag{4.35}$$

which needs to be solved for B, if the next order is required.

4.5. *Matching*

Finally we want to calculate the missing coefficients in the expression (4.28) for $\dot{\theta}$, also including the correction $t^{-2/3}$ from (4.34). We do that by matching the missing amplitudes and phases of the successive regions, starting from (4.14). First, the limit of the intermediate solution (4.33) for $s \to 0$ (toward the right end) is

$$\Delta\kappa = 4A_{med} e^{-\frac{3}{2}\left(1 \pm \sqrt{3}i\right)(\zeta/4)^{4/3}} s^{-4/3} t^{5/6}, \quad \zeta = \frac{1-x}{t^{1/4}};$$

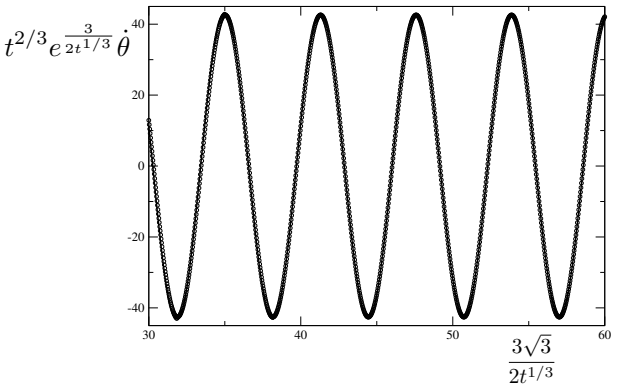

FIGURE 8. The change in contact angle $\dot{\theta}$ as obtained from a numerical simulation of (4.1) (solid line), compared to the prediction (4.40); a best fit (symbols) gives $t^{2/3}e^{3/(2t^{1/3})}\dot{\theta} = -42.6\cos\left(\frac{3\sqrt{3}}{2t^{1/3}} - 0.4625\right)$.

comparison to (4.13) yields $A_{med} = A_p/4$, and including the phase factor we have for the real version of the intermediate solution

$$\Delta\kappa = \frac{A_p}{4}\frac{1+x^{1/4}+x^{1/2}+x^{3/4}}{x^{9/8}(1-x)^{4/3}}t^{5/6}e^{-\frac{3}{2}\frac{(1-x^{1/4})^{4/3}}{t^{1/3}}}\cos\left(\frac{3\sqrt{3}}{2t^{1/3}}\left(1-x^{1/4}\right)^{4/3} - \phi_p\right). \tag{4.36}$$

Thus the expression for the overlap region between (4.36) and (4.14) is

$$\Delta\kappa = \frac{A_p t^{5/6}}{s^{4/3}}e^{-\frac{3\zeta^{4/3}}{2\cdot 4^{4/3}}}\cos\left(\frac{3\sqrt{3}\zeta^{4/3}}{2\cdot 4^{4/3}} - \phi_p\right). \tag{4.37}$$

In the opposite limit $x \to 0$ (near the contact line), the intermediate solution (4.36) becomes (note that $f(x) \approx x^{-9/8}$):

$$\Delta\kappa = \frac{A_p}{4}x^{-9/8}t^{5/6}e^{-\frac{3}{2t^{1/3}}(1-4x^{1/4}/3)}\cos\left(\frac{3\sqrt{3}}{2t^{1/3}}\left(1-\frac{4}{3}x^{1/4}\right) - \phi_p\right). \tag{4.38}$$

Now (4.38) can be compared to the large-ξ limit of (4.27), but including the factor $t^{-2/3}$ implied by the leading order contribution to (4.27). This shows that $\epsilon_1 = \epsilon\cos\phi_p$ and $\epsilon_2 = -\epsilon\sin\phi_p$, with $\epsilon = -\sqrt{\pi}A_p t^{-2/3}/\sqrt{2}$. Inserting this into (4.27), including the factor of $t^{-2/3}$, we arrive at the complete solution for the contact line region:

$$\Delta\kappa = -\sqrt{\frac{\pi}{2}}\frac{A_p}{t^{2/3}}e^{-3/(2t^{1/3})}\left[\cos\left(\frac{3\sqrt{3}}{2t^{1/3}} - \phi_p\right)A_r + \sin\left(\frac{3\sqrt{3}}{2t^{1/3}} - \phi_p\right)A_i\right], \tag{4.39}$$

where

$$A_r + iA_i = \text{MeijerG}\left([[],[]],[[0,0],[-2,-1]],-\frac{(1+\sqrt{3}i)\xi}{2}\right), \quad \xi = \frac{x}{t^{4/3}}.$$

Now we can deduce the change in contact angle by taking the small-ξ limit of (4.39), keeping the logarithmically diverging terms only, to obtain

$$\Delta\kappa \approx \frac{A_p\sqrt{\pi}}{2\sqrt{2}}t^{-2/3}e^{-3/(2t^{1/3})}\cos\left(\frac{3\sqrt{3}}{2t^{1/3}} - \phi_p\right)\ln x \equiv 2b\ln x.$$

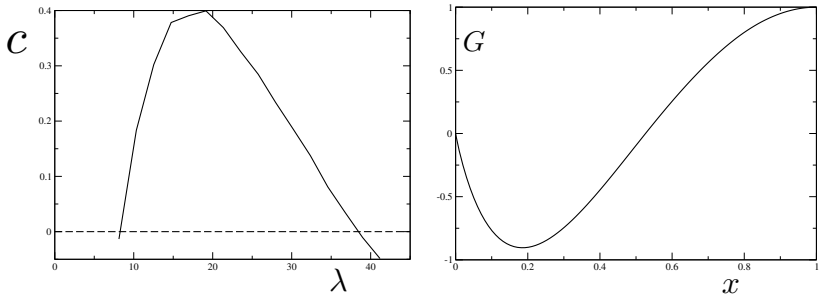

FIGURE 9. Left: The constant c, as defined in (5.3), as a function of λ. Zeroes determine the eigenvalues - the first two are shown, with $\lambda_1 = 8.19$ and $\lambda_2 = 38.4$, based on $V = 2/3$. Right: the first eigenfunction $G_1(x)$, corresponding to λ_1.

According to (3.5), $\dot{\theta} = -4b$, and thus

$$\dot{\theta} = -\frac{A_p\sqrt{\pi}}{\sqrt{2}} t^{-2/3} e^{-3/(2t^{1/3})} \cos\left(\frac{3\sqrt{3}}{2t^{1/3}} - \phi_p\right), \tag{4.40}$$

which is the final desired equation of motion for the contact angle. In Fig. 8 the functional form of (4.40) is compared to numerical solutions of the linearized problem (4.1), from which $\dot{\theta}$ is obtained; almost perfect agreement is found. Using that $A_p = 51.39$ as found from the pulse solution, the predicted prefactor is 64.4, while a prefactor of 42.6 is found numerically. The slight disagreement comes from the fact that convergence is slow, so $t \sim 10^{-4}$ is not yet asymptotic. Accessing earlier times numerically is difficult, since this would require an even greater range of spatial scales to be resolved with great accuracy. The observed phase factor of 0.4625 is also in reasonable agreement with the prediction of $\phi_p = 0.561$, once more found from the pulse solution.

5. Long time evolution

We investigate small perturbations to (2.3), in order to describe the relaxation toward the equilibrium shape:

$$h = h_{eq} + \epsilon e^{-\lambda t} G(x). \tag{5.1}$$

Inserting into (1.1) and linearizing results in ϵ we find the eigenvalue equation

$$\lambda G = \left(h_{eq}^3 G_{xxx}\right)_x, \tag{5.2}$$

an ODE of fourth order. We need to find a solution to (5.2) that satisfies the boundary condition $G(0) = 0$. Solving (5.2) by shooting, we use the initial conditions $G(1) = 1$ (a normalization), $G'(1) = G'''(1) = 0$ (symmetry), and $G''(1) = \psi$, where ψ is a shooting parameter. For a generic value of ψ, G behaves like

$$G \approx d\ln x + c - d\lambda x \ln^2 x/2 + (d-c)\lambda x \ln(x) + \ldots, \tag{5.3}$$

near $x = 0$, as found by expanding G in x and $\ln x$.

To find the eigenfunction, we first adjust ψ such that the diverging term $d\ln x$ disappears, which is done by demanding that $G'x \to 0$ for $x \to 0$. Next, we plot $G(0)$ or c as a function of λ, see the left of Fig. 9; the condition $c = G(1) = 0$ determines the eigenvalue, since this is the boundary condition G has to satisfy at the contact line. We have chosen $V = 2/3$, the result for arbitrary volume is found from rescaling. On the left of Fig. 9, the range of λ shown includes the first two zeroes of $G(0)$, corresponding to

the first two eigenvalues. On the right of Fig. 9, we show the first eigenfunction $G_1(x)$, corresponding to $\lambda_1 = 8.19$. Clearly, the eigenvalue scales with V^3, so that the decay exponent in Fig.2 is

$$\lambda = (3V/2)^3\lambda_1 = (6\bar{h}/\pi)^3\lambda_1 = 0.057.$$

The resulting decay law $\dot{\theta} \propto e^{-t/\lambda}$ (with the prefactor adjusted) is shown as the dashed line, and fits the observed decay (solid line) very well.

From (5.1) if follows that $\dot{\theta} = -\epsilon\lambda G'(0)e^{-\lambda t}$. Since $G_1'(0) \approx -14.05$ is finite, it follows that the contact angle is changing as $t \to \infty$. Alternatively, $\dot{\theta}$ can be calculated from (2.2). With the coefficients c, d in (5.3) having been made to vanish, the local expansion of G_1 becomes

$$G_1(x) = ax + \frac{a\lambda_1}{4}x^2 \ln x + \dots.$$

As shown on the left of Fig.9, the next eigenvalue λ_2 is significantly larger than λ_1, so the first eigenvalue will dominate for times of order unity.

6. Discussion

The problem considered in this paper was motivated originally by discussions at the workshop "Analysis and numerics of nonlinear PDEs: degeneracies & free boundaries", held in 2023 at the Lorentz center in Leiden (Gnann *et al.* 2023). The aim was to find a mathematical framework for the contact line paradox which concludes that in the case of the standard formulation of fluid mechanics, with no slip at solid boundaries, a contact line cannot move (Huh & Scriven 1971; Dussan V. & Davis 1974). In (1.1), and of course allowing for the thin film approximation being applicable, this means that $n = 3$. On dimensional grounds, any other exponent requires the existence of another length scale, such as a slip length.

The argument (Giacomelli *et al.* 2023) proceeds from assuming a (potentially mobile) contact line at position $s(t)$, where $h(x, t)$ satisfies the boundary conditions

$$h(s, t) = 0, \quad h_x(s, t) = 1; \tag{6.1}$$

the contact angle has been normalized to unity. Then contact line motion consistent with (1.1) must satisfy

$$\lim_{x\to s} h^{n-1}h_{xxx} = \dot{s}(t). \tag{6.2}$$

Now assume a classical solution to (1.1) with $n = 3$ and boundary conditions (6.1), with contact line motion defined by (6.2). It follows that $\dot{s} = 0$; we show this by contradiction. Assume that on the contrary $\dot{s} \neq 0$. Then since $h \approx x' = x - s$ near the contact line, we have $h_{xxx} \approx \dot{s}/x'^2$. Integrating, it follows that $h_x \approx -\dot{s} \ln x'$, which contradicts $h_x(s) = 1$. Thus our assumption of $\dot{s} \neq 0$ must have been incorrect, and we have shown that $\dot{s} = 0$ instead. Note that we have not used the equation of motion (1.1) to reach this conclusion.

In other words, for $n = 3$ the contact line is effectively pinned, even though we have not introduced explicit pinning forces. Thus we can conclude from our results (e.g. (4.40)) that the contact angle will change instantaneously, unless the initial condition is an equilibrium profile. But since we also have to satisfy the second condition of (6.1), which fixes the contact angle, we see that there are *too many* boundary conditions to be satisfied. This means the contact line problem with $n = 3$ is *ill-posed*, and there is no solution. This result is fascinating, in that it implies that a pure continuum description, which does not introduce a microscopic length scale, is inherently inconsistent, regardless of

any experimental evidence for the motion of contact lines. This comes as close as one possibly can to proving the existence of atoms by purely mathematical means!

A remaining question is what might be a convenient method to observe the motion of pinned drops as described here. Placing the drop on a substrate might result in a rather ill-controlled initial state. By contrast, using electrical forces to move drops already on the substrate might be a more convenient way, including the use of electrically tunable defects to trap a drop initially ('t Mannetje *et al.* 2014).

Declaration of Interests. The authors report no conflict of interest.

Acknowledgments

M. A. F. acknowledges financial support through project TED2021-131530B-I00. We are grateful to L. Giacomelli, H. Knüpfer, and J.J.L. Velázquez for inspiring discussions.

Appendix A. The local solution, $\delta \neq 0$

The four linearly independent solutions of (3.9) are

$$P_1 = {}_1F_3\left(-\frac{1}{1+\delta}; \frac{1}{1+\delta}, \frac{3}{1+\delta}, \frac{2}{1+\delta}, \frac{\xi^{1+\delta}}{(1+\delta)^4}\right), \tag{A 1}$$

$$P_2 = {}_1F_3\left(\frac{-2+\delta}{1+\delta}; \frac{\delta}{1+\delta}, \frac{2\delta}{1+\delta}, \frac{2+\delta}{1+\delta}, \frac{\xi^{1+\delta}}{(1+\delta)^4}\right)\xi^{\delta-1}, \tag{A 2}$$

$$P_3 = {}_1F_3\left(\frac{-1+\delta}{1+\delta}; \frac{2+\delta}{1+\delta}, \frac{1+2\delta}{1+\delta}, \frac{3+\delta}{1+\delta}, \frac{\xi^{1+\delta}}{(1+\delta)^4}\right)\xi^{\delta}, \tag{A 3}$$

$$P_4 = {}_1F_3\left(\frac{-3+\delta}{1+\delta}; \frac{\delta}{1+\delta}, \frac{-1+2\delta}{1+\delta}, \frac{-1+\delta}{1+\delta}, \frac{\xi^{1+\delta}}{(1+\delta)^4}\right)\xi^{\delta-2}, \tag{A 4}$$

only P_1 and P_3 being compatible with (3.7). We will assume $\delta > 0$ for the following calculation; the opposite case is similar.

Using contour integration in the complex plane, we can express our functions by means of Barnes-type integrals:

$$P_1 = \frac{1}{2\pi i}\frac{\Gamma(\frac{1}{1+\delta})\Gamma(\frac{2}{1+\delta})\Gamma(\frac{3}{1+\delta})}{\Gamma(-\frac{1}{1+\delta})}\int_{-\varepsilon-i\infty}^{-\varepsilon+i\infty}\frac{\Gamma(s-\frac{1}{1+\delta})\Gamma(-s)}{\Gamma(s+\frac{1}{1+\delta})\Gamma(s+\frac{2}{1+\delta})\Gamma(s+\frac{3}{1+\delta})}\left(-\frac{\xi^{1+\delta}}{(1+\delta)^4}\right)^s ds$$
$$-e^{\frac{1}{1+\delta}\pi i}\frac{\Gamma(\frac{1}{1+\delta})}{\Gamma(\frac{4}{1+\delta})}\frac{\xi}{(1+\delta)^{\frac{4}{1+\delta}}},$$

$$P_3 = \frac{1}{2\pi i}\frac{\Gamma(\frac{1+2\delta}{1+\delta})\Gamma(\frac{2+\delta}{1+\delta})\Gamma(\frac{3+\delta}{1+\delta})}{\Gamma(\frac{-1+\delta}{1+\delta})}\int_{-\varepsilon-i\infty}^{-\varepsilon+i\infty}\frac{\Gamma(s+\frac{-1+\delta}{1+\delta})\Gamma(-s)}{\Gamma(s+\frac{1+2\delta}{1+\delta})\Gamma(s+\frac{2+\delta}{1+\delta})\Gamma(s+\frac{3+\delta}{1+\delta})}\left(-\frac{\xi^{1+\delta}}{(1+\delta)^4}\right)^s \xi^{\delta} ds$$
$$-e^{\frac{1-\delta}{1+\delta}\pi i}\frac{\Gamma(\frac{1+2\delta}{1+\delta})\Gamma(\frac{2+\delta}{1+\delta})\Gamma(\frac{3+\delta}{1+\delta})}{\Gamma(\frac{2+\delta}{1+\delta})\Gamma(\frac{3}{1+\delta})\Gamma(\frac{4}{1+\delta})}\frac{\xi}{(1+\delta)^{4\frac{1-\delta}{1+\delta}}}.$$

The two solutions can be combined in the form

$$P_3 - rP_1 = \Re(P_3 - rP_1) =$$
$$\Re\left(-e^{\frac{1-\delta}{1+\delta}\pi i}\frac{\Gamma(\frac{1+2\delta}{1+\delta})\Gamma(\frac{2+\delta}{1+\delta})\Gamma(\frac{3+\delta}{1+\delta})}{\Gamma(\frac{2+\delta}{1+\delta})\Gamma(\frac{3}{1+\delta})\Gamma(\frac{4}{1+\delta})(1+\delta)^{4\frac{1-\delta}{1+\delta}}} + re^{\frac{1}{1+\delta}\pi i}\frac{\Gamma(\frac{1}{1+\delta})}{\Gamma(\frac{4}{1+\delta})(1+\delta)^{\frac{4}{1+\delta}}}\right)\xi + \Re(Q_3 - rQ_1),$$

where

$$Q_1 = \frac{\Gamma(\frac{1}{1+\delta})\Gamma(\frac{2}{1+\delta})\Gamma(\frac{3}{1+\delta})}{2\pi i\Gamma(-\frac{1}{1+\delta})}\int_{-\varepsilon-i\infty}^{-\varepsilon+i\infty}\frac{\Gamma(s-\frac{1}{1+\delta})\Gamma(-s)}{\Gamma(s+\frac{1}{1+\delta})\Gamma(s+\frac{2}{1+\delta})\Gamma(s+\frac{3}{1+\delta})}\left(-\frac{\xi^{1+\delta}}{(1+\delta)^4}\right)^s ds,$$

$$Q_3 = \frac{\Gamma(\frac{1+2\delta}{1+\delta})\Gamma(\frac{2+\delta}{1+\delta})\Gamma(\frac{3+\delta}{1+\delta})}{2\pi i\Gamma(\frac{-1+\delta}{1+\delta})}(1+\delta)^{\frac{4\delta}{1+\delta}}\int_{-\varepsilon-i\infty}^{-\varepsilon+i\infty}\frac{e^{\pi i\frac{\delta}{1+\delta}}\Gamma\left(s-\frac{1}{1+\delta}\right)\Gamma(-s+\frac{\delta}{1+\delta})}{\Gamma(s+1)\Gamma(s+\frac{2}{1+\delta})\Gamma(s+\frac{3}{1+\delta})}\left(-\frac{\xi^{1+\delta}}{(1+\delta)^4}\right)^s ds.$$

By choosing

$$r = \frac{-2\delta\Gamma^2(\frac{\delta}{1+\delta})\,(1+\delta)^{\frac{4\delta}{1+\delta}}}{(2-\delta)(1-2\delta)\Gamma(\frac{-1+\delta}{1+\delta})\Gamma(\frac{1-2\delta}{1+\delta})}, \tag{A 5}$$

we have

$$Q_3 - rQ_1 = \frac{1}{2\pi i}\frac{\Gamma(\frac{1}{1+\delta})\Gamma(\frac{2}{1+\delta})\Gamma(\frac{3}{1+\delta})}{\Gamma(-\frac{1}{1+\delta})}\times$$
$$\int_C \frac{\Gamma(s-\frac{1}{1+\delta})}{\Gamma(s+\frac{2}{1+\delta})\Gamma(s+\frac{3}{1+\delta})}\left[\frac{e^{\pi i\frac{\delta}{1+\delta}}\Gamma(-s+\frac{\delta}{1+\delta})}{\Gamma(s+1)} - \frac{\Gamma(-s)}{\Gamma(s+\frac{1}{1+\delta})}\right]\left(-\frac{\xi^{1+\delta}}{(1+\delta)^4}\right)^s ds,$$

where the term in brackets has good decay properties at infinity owing to

$$\Gamma(-s)\Gamma(s+1) = -\frac{\pi}{\sin(\pi s)}, \quad \Gamma(-s+\frac{\delta}{1+\delta})\Gamma(s+\frac{1}{1+\delta}) = -\frac{\pi}{\sin(\pi(s-\frac{\delta}{1+\delta}))},$$

so that $\Re(Q_3 - rQ_1)$ is bounded.

Finally, the slope of the linear behavior is found to be

$$sl = \Re(sl) = -\frac{\Gamma(\frac{1+2\delta}{1+\delta})\Gamma(\frac{2+\delta}{1+\delta})\Gamma(\frac{3+\delta}{1+\delta})}{\Gamma(\frac{3}{1+\delta})\Gamma(\frac{4}{1+\delta})}\frac{1}{(1+\delta)^{4\frac{1-\delta}{1+\delta}}}\Re\left(\frac{\Gamma(-\frac{1}{1+\delta})}{\Gamma(\frac{-1+\delta}{1+\delta})\Gamma(\frac{2}{1+\delta})}e^{\frac{1}{1+\delta}\pi i} - e^{\frac{1-\delta}{1+\delta}\pi i}\frac{1}{\Gamma(\frac{2+\delta}{1+\delta})}\right),$$

from which we find

$$P_0 = \frac{6\cdot 16^{\frac{1}{1+\delta}}\left(1-\cos\left(\frac{2\pi(2+\delta)}{1+\delta}\right)\right)\Gamma\left(\frac{5+\delta}{2+2\delta}\right)\Gamma\left(\frac{3}{1+\delta}\right)\Gamma\left(\frac{2+\delta}{1+\delta}\right)}{\delta\pi^{\frac{3}{2}}\,(1+\delta)^{\frac{\delta-7}{1+\delta}}\left(\sin\left(\frac{\pi}{1+\delta}\right)+6\sin\left(\frac{\pi\delta}{1+\delta}\right)-\sin\left(\frac{\pi(1+2\delta)}{1+\delta}\right)\right)}. \tag{A 6}$$

For general n, the two solutions to (3.15) with the correct behavior at infinity are

$$P_1 = {}_1\mathrm{F}_3\left(-\frac{n-2}{1+\delta};\frac{1}{1+\delta},\frac{3}{1+\delta},\frac{2}{1+\delta},\frac{\xi^{1+\delta}}{(1+\delta)^4}\right),$$
$$P_3 = {}_1\mathrm{F}_3\left(\frac{2+\delta-n}{1+\delta};\frac{2+\delta}{1+\delta},\frac{1+2\delta}{1+\delta},\frac{3+\delta}{1+\delta},\frac{\xi^{1+\delta}}{(1+\delta)^4}\right)\xi^\delta. \tag{A 7}$$

The remaining calculation can be done similarly to the above.

Appendix B. The pulse solution, $\delta = 0$

Any solution to (4.10) can be written as a linear superposition of the four solutions

$$\phi_1 = {}_1\mathrm{F}_3\left(-\frac{1}{4};\frac{1}{2},\frac{3}{4},\frac{5}{4},\frac{\zeta^4}{256}\right)\zeta,\ \phi_2 = {}_1\mathrm{F}_3\left(-\frac{1}{4};\frac{5}{4},\frac{3}{2},\frac{7}{4},\frac{\zeta^4}{256}\right)\zeta^3,$$
$$\phi_3 = {}_1\mathrm{F}_3\left(-\frac{1}{2};\frac{1}{4},\frac{1}{2},\frac{3}{4},\frac{\zeta^4}{256}\right),\ \phi_4 = \zeta^2, \tag{B 1}$$

where ${}_p\mathrm{F}_q$ denotes the generalized hypergeometric function. Writing $\phi_1 = \zeta P_1$ and $\phi_2 = \zeta^3 P_2$, the first two solutions can be represented as integrals:

$$P_1 = \frac{1}{2\pi i}\frac{\Gamma\left(\frac{1}{2}\right)\Gamma\left(\frac{3}{4}\right)\Gamma\left(\frac{5}{4}\right)}{\Gamma\left(-\frac{1}{4}\right)}\int_{L_1}\frac{\Gamma\left(-\frac{1}{4}-s\right)}{\Gamma\left(\frac{1}{2}-s\right)\Gamma\left(\frac{3}{4}-s\right)\Gamma\left(\frac{5}{4}-s\right)}\Gamma(s)\left(-\left(\frac{\zeta}{4}\right)^4\right)^{-s}ds,$$

where L_1 separates the poles of $\Gamma\left(-\frac{1}{4}-s\right)$ and $\Gamma(s)$, and

$$P_2 = \frac{1}{2\pi i}\frac{\Gamma\left(\frac{5}{4}\right)\Gamma\left(\frac{3}{2}\right)\Gamma\left(\frac{7}{4}\right)}{\Gamma\left(\frac{1}{4}\right)}\int_{L_2}\frac{\Gamma\left(\frac{1}{4}-s\right)}{\Gamma\left(\frac{5}{4}-s\right)\Gamma\left(\frac{3}{2}-s\right)\Gamma\left(\frac{7}{4}-s\right)}\Gamma(s)\left(-\left(\frac{\zeta}{4}\right)^4\right)^{-s}ds,$$

where L_2 separates the poles of $\Gamma\left(\frac{1}{4}-s\right)$ and $\Gamma(s)$.

We observe that

$$\begin{aligned}\zeta^2 P_2 &= 16\frac{1}{2\pi i}\frac{\Gamma\left(\frac{5}{4}\right)\Gamma\left(\frac{3}{2}\right)\Gamma\left(\frac{7}{4}\right)}{\Gamma\left(\frac{1}{4}\right)}\int_{L_2}\frac{\Gamma\left(\frac{1}{4}-s\right)}{\Gamma\left(\frac{5}{4}-s\right)\Gamma\left(\frac{3}{2}-s\right)\Gamma\left(\frac{7}{4}-s\right)}\Gamma(s)\left(-\left(\frac{\zeta}{4}\right)^4\right)^{-s+\frac{1}{2}}ds\\ &= 16\frac{1}{2\pi i}\frac{\Gamma\left(\frac{5}{4}\right)\Gamma\left(\frac{3}{2}\right)\Gamma\left(\frac{7}{4}\right)}{\Gamma\left(\frac{1}{4}\right)}\int_{L_1}\frac{\Gamma\left(-\frac{1}{4}-s\right)}{\Gamma\left(\frac{3}{4}-s\right)\Gamma(1-s)\Gamma\left(\frac{5}{4}-s\right)}\Gamma(s+\frac{1}{2})\left(-\left(\frac{\zeta}{4}\right)^4\right)^{-s}ds,\end{aligned}$$

so that we can combine the two solutions as

$$\begin{aligned}P_1 - r\zeta^2 P_2 = \frac{1}{2\pi i}&\frac{\Gamma\left(\frac{1}{2}\right)\Gamma\left(\frac{3}{4}\right)\Gamma\left(\frac{5}{4}\right)}{\Gamma\left(-\frac{1}{4}\right)}\times\\ \int_L\frac{\Gamma\left(-\frac{1}{4}-s\right)}{\Gamma\left(\frac{3}{4}-s\right)\Gamma\left(\frac{5}{4}-s\right)}&\left[\frac{\Gamma(s)}{\Gamma\left(\frac{1}{2}-s\right)} - 6r\frac{\Gamma\left(-\frac{1}{4}\right)}{\Gamma\left(\frac{1}{4}\right)}\frac{\Gamma(s+\frac{1}{2})}{\Gamma(1-s)}\right]\left(-\left(\frac{\zeta}{4}\right)^4\right)^{-s}ds.\end{aligned}$$

The parameter

$$r = \frac{\Gamma\left(\frac{1}{4}\right)}{6\Gamma\left(-\frac{1}{4}\right)} = \frac{\sqrt{2}\pi}{24\Gamma^2\left(\frac{3}{4}\right)} \tag{B 2}$$

has to be chosen such that the square brackets cancel for $s \to \pm i\infty$. To find the linear behavior of the resulting expression for large ζ, we calculate the residual of the integral at the pole $s = -1/4$ to yield

$$P_1 - r\zeta^2 P_2 \sim -\frac{4\pi}{\Gamma\left(-\frac{1}{4}\right)}\frac{\zeta}{4} = \frac{\pi}{\Gamma\left(\frac{3}{4}\right)}\frac{\zeta}{4},\ \text{as } \zeta\to\infty.$$

Appendix C. The contact line solution solution, $\delta = 0$

Four linearly independent solutions of (4.17) are

$$\begin{gathered}A_1 = \mathrm{MeijerG}([[],[]],[[0,0],[-2,-1]],-\mu\xi),\ A_2 = {}_0\mathrm{F}_3(1,2,3,-\mu\xi),\\ A_3 = \mathrm{MeijerG}([[],[]],[[-1,0,0],[-2]],-\mu\xi),\ A_4 = \mathrm{MeijerG}([[],[]],[[-2,-1,0,0],[]],-\mu\xi).\end{gathered} \tag{C 1}$$

For simplicity, in the following we assume that $\mu = (1+i\sqrt{3})/2$. Then the asymptotic behavior of A_2 for large ξ is

$$A_2 \approx -\frac{1-i}{4\pi^{3/2}}e^{-4i\mu\xi^{1/4}}\xi^{-9/8}. \tag{C 2}$$

Including corrections, the asymptotic behavior of A_1 is

$$A_1 \approx -\frac{\sqrt{2}}{4\sqrt{\pi}} e^{4\mu\xi^{1/4}} \xi^{-9/8} \left[1 - \frac{39}{32}\bar{\mu}\xi^{-1/4} - \frac{1593}{2048}\mu\xi^{-1/2} + O(\xi^{-3/4})\right]. \tag{C 3}$$

Note that the current implementation of Mathematica, as well as the documentation, contains an erroneous factor of 1/2 relative to (C 3). This is confirmed against the theory presented in (Braaksma 1962); in the notation of this paper, we have $q = 4, p = 0, m = 2$, and $n = 0$. Using Theorem 12 and (4.13) of (Braaksma 1962), we find

$$A_1 \sim \lambda_{-2} E(z) \sim \lambda_{-2} A_0 (4^4 z)^{-9/8} e^{4z^{1/4}},$$

where λ_{-2} and A_0 follow from (11.17) and (3.28), respectively, to give

$$A_1 \sim \frac{(2\pi i)^2 e^{3\pi i} 4^5}{4(2\pi i)(2\pi)^{3/2}(4^4 z)^{9/8}} e^{4z^{1/4}}.$$

Now putting $z = -\mu\xi$, we confirm the leading term of (C 3). We have also checked against the numerical implementations of the MeijerG functions in Mathematica and in Maple.

To find the asymptotic behavior for small ξ, we note that the MeijerG functions can be written as Mellin transforms, so that the first solution of (C 1) (the only one relevant to our solution), can be written as

$$A_1(\xi) = \frac{1}{2\pi i} \int \frac{\Gamma^2(s)}{\Gamma(2-s)\Gamma(3-s)} (-\mu\xi)^{-s} ds. \tag{C 4}$$

On the basis of this representation, an asymptotic description can be found using the residue theorem (with $a \equiv -\mu\xi$):

$$A_1(\xi) = \sum_{n=0}^{\infty} \mathrm{Res}\left(\frac{\Gamma^2(s) a^{-s}}{\Gamma(2-s)\Gamma(3-s)}, s = -n\right) =$$
$$\sum_{n=0}^{\infty} a^n \mathrm{Res}\left(\frac{\Gamma^2(s'-n) a^{-s'}}{\Gamma(2+n-s')\Gamma(3+n-s')}, s' = -0\right),$$

which has the form of an expansion for small a. On account of the Γ function factors, the series is convergent for all a.

By contrast, the corresponding integral representations for A_3 and A_4 show that $A_3 \sim \xi^{-1}$, and $A_4 \sim \xi^{-2}$; they are singular at the origin and thus do not need to be considered. Now A_1 is of the form

$$A_1 = \sum_{n=0}^{\infty} a^n \left(c_0(n) + c_1(n) \ln a\right), \tag{C 5}$$

with

$$c_0 = \frac{4(2+n)^2(1+n)\left[\left(n^3+3n^2+2n\right)\Psi(n) + 7n^2/4 + 17n/4 + 2\right]}{n\Gamma^4(3+n)},$$

and $c_1 = -(1+n)^2(2+n)^3/\Gamma^4(3+n)$. The contribution proportional to $\ln a$ can be summed to give

$$\sum_{n=0}^{\infty} a^n c_1(n) = -\frac{1}{2}\mathrm{F}(1,2,3,a) = -\frac{1}{2}A_2.$$

Evaluating the sum up to second order, we find

$$A_1 = \frac{5}{4} - 2\gamma - \frac{\ln a}{2} - \frac{a}{24}\left(-\frac{32}{3} + 8\gamma + 2\ln(a)\right) + O(a^2, a^2 \ln a). \tag{C 6}$$

REFERENCES

Bonn, D., Eggers, J., Indekeu, J., Meunier, J. & Rolley, E. 2009 Wetting and spreading. *Rev. Mod. Phys.* **81**, 739–805.

Braaksma, B. L. J. 1962 Asymptotic expansions and analytic continuations for a class of Barnes-integrals. *Compositio Mathematica* **15**, 239.

de Gennes, P.-G. 1985 Wetting: statics and dynamics. *Rev. Mod. Phys.* **57**, 827–863.

Dupont, T. F., Goldstein, R. E., Kadanoff, L. P. & Zhou, S.-M. 1993 Finite-time singularity formation in Hele-Shaw systems. *Phys. Rev. E* **47**, 4182.

Dussan V., E. B. & Chow, R. T.-P. 1983 On the ability of drops or bubbles to stick to non-horizintal surfaces of solids. *J. Fluid Mech.* **137**, 1–29.

Dussan V., E. B. & Davis, S. H. 1974 On the motion of a fluid-fluid interface along a solid surface. *J. Fluid Mech.* **65**, 71–95.

Eggers, J. & Fontelos, M. A. 2015 *Singularities: Formation, Structure, and Propagation*. Cambridge University Press, Cambridge.

Giacomelli, L., Knüpfer, H. & Velázquez, J. J. L. 2023 private communication.

Gnann, M., Giacomelli, L., Lienstromberg, C., Hulshof, J. & Sonner, S. 2023 Analysis and numerics of nonlinear pdes: degeneracies & free boundaries. Lorentz center, Leiden.

Graña-Otero, J. & Parra Fabián, I. E. 2019 Contact line depinning from sharp edges. *Phys. Rev. Fluids* **4**, 114001.

Hong, S. H., Fontelos, M. A. & Hwang, H. J. 2016 The contact line of an evaporating droplet over a solid wedge and the pinned-unpinned transition. *J. FLuid Mech.* **791**, 519.

Huh, C. & Scriven, L. E. 1971 Hydrodynamic model of steady movement of a solid/liquid/fluid contact line. *J. Coll. Int. Sci.* **35**, 85–101.

Oron, A., Davis, S. H. & Bankoff, S. G. 1997 Long-scale evolution of thin liquid films. *Rev. Mod. Phys.* **69**, 931–980.

Quéré, D., Lafuma, A. & Bico, J. 2003 Slippy and sticky microtextured solids. *Nanotechnology* **14**, 1109.

Stone, H. A. & Duprat, C. 2016 *Fluid-Structure Interactions in Low-Reynolds-Number Flows*, chap. 3, pp. 77–99. Royal Society of Chemistry.

Wilson, S. K. & D'Ambrosio, H-M 2023 Evaporation of sessile droplets. *Annu. Rev. Fluid Mech.* **55**, 481–509.

't Mannetje, D., Ghosh, S., Lagraauw, R., Otten, S., Pit, A., Berendsen, C., Zeegers, J., van den Ende, D. & Mugele, F. 2014 Trapping of drops by wetting defects. *Nature Comm.* **5**, 3559.